Asian Journal of Green Chemistry

Original Research Article View Article Online | View Journal

Extraction of Cellulose from Bagasse for the Synthesis of Alginate:Cellulose Porous Beads

Eny Yulianti[1], Lilik Miftahul Khoiroh[1], Rif'atul Mahmudah[1], Sindi Puspitasari[1], Faiqotul Himmah[1], Tzu-Teng Huang[2], Imtiaz Ali Laghari[3], Ahmad Zikri[4], Mohammad Abdullah[5], Rahadian Zainul[6,7]*, Tarek A. Elkhooly[8,9]

[1]*Department of Chemistry, Faculty of Science and Technology, UIN Maulana Malik Ibrahim Malang Jalan Gajayana 50, Malang 65144, East Java, Indonesia*
[2]*Department of Mechanical Engineering, National Cheng Kung University (NCKU), Tainan, Taiwan*
[3]*Department of Electrical Engineering, Quaid-e-Awam University of Engineering, Science and Technology, Campus Larkana, Sindh 67480, Pakistan*
[4]*Department of Mechanical Engineering, Faculty of Engineering, Bursa Uludag University, Bursa 16850, Türkiye*
[5]*Chemical Engineering Studies, College of Engineering, Universiti Teknologi MARA Johor Branch, Pasir Gudang Campus, Bandar Seri Alam, 81750 Masai, Pasir Gudang, Johor Bahru, Johor, Malaysia*
[6]*Department of Chemistry, Faculty of Mathematics and Natural Sciences, Universitas Negeri Padang, Padang, West Sumatra, Indonesia*
[7]*Center for Advanced Material Processing, Artificial Intelligence and Biophysics Informatics (CAMPBIOTICS), Universitas Negeri Padang, Indonesia*
[8]*Nanomedicine Research Unit, Faculty of Medicine, Delta University for Science and Technology, Gamasa 11152, Egypt*
[9]*Department of Refractories, Ceramics and Building Materials, National Research Centre, Giza, 12622, Egypt*

ARTICLE INFORMATION

Submitted: 2024-01-09
Revised: 2024-02-20
Accepted: 2024-02-20
Manuscript ID: AJGC-2401-1475
Checked for Plagiarism: Yes
Language Editor Checked: Yes

DOI: 10.48309/AJGC.2024.440660.1475

KEYWORDS

Bagasse
Cellulose beads
Alginate
Beads
Cross-linked

ABSTRACT

This study aimed to develop the production of porous cellulose beads from bagasse. Alkali extraction with 6% sodium hydroxide was identified as the optimal solvent for cellulose, based on the swelling ratio. This process resulted in viscose cellulose solution with improved characteristics, including a density of 1.099 g/ml, viscosity of 0.024 Pa·s, molecular weight of 171.668 g/mol, and a swelling ratio of 50.8%. The beads fabrication using the cellulose extract combined with alginate led to the formation of beads with a homogeneous and rough surface. Calcium carbonate ($CaCO_3$) was utilized as a porogen and zinc acetate served as the crosslinking agent. The optimal composition of alginate to cellulose xanthate for bead formation, determined through evaluations of bead geometry, swelling power, and surface porosity using SEM-EDX, was found to be a 2:2 ratio.

Corresponding authors, email: rahadianzmsiphd@fmipa.unp.ac.id (R. Zainul).
Tel.: 6281261385385.

Graphical Abstract

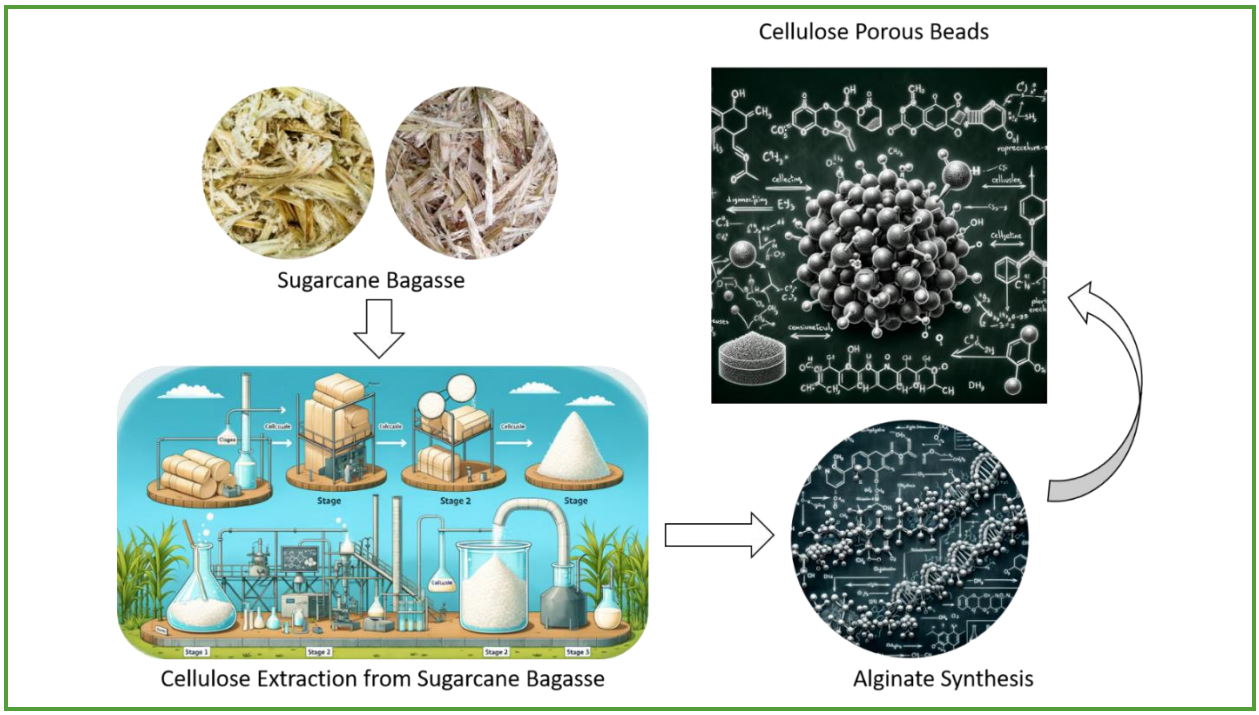

Introduction

Bagasse from sugarcane mills is a significant agricultural waste, still containing 50% cellulose [1-4]. Cellulose, a polymer made of glucose, consists of β-1,4-glucoside units linked in a straight, unbranched chain. This structure contributes to its slight stiffness [5-8]. Widely used in various industries, cellulose serves as an adsorbent, drug carrier, and food additive. It is valued both in its natural form and when chemically modified to create derivatives [9-11]. Cellulose stands out as an adsorbent for several reasons: it is renewable, degradable, and can be modified to meet specific needs [12-14]. To enhance its physical and chemical properties and widen its applications, cellulose is converted into various derivatives, such as cellulose xanthate [15-17]. This particular derivative is non-flammable and exhibits higher crystallinity than natural cellulose [18, 19]. The process to produce cellulose xanthate involves reacting alkaline cellulose with carbon disulfide (CS_2) [20-22].

Beads, or spherical microcapsules, are prepared as coated or encapsulated solid substrates [23-26]. They feature a uniform particle size distribution, highly porous structures, high surface area, chemical reactivity, and mechanical strength [27-30]. Beads made from the biopolymers alginate and cellulose are more effective in adsorption than flakes, due to their higher adsorption capacity [31-34] and larger surface area [35-37]. One common method for forming beads is ionic gelation [38-40]. This method utilizes a cross-linking reaction between a polyelectrolyte [41, 42] and its multivalent ion pair, enhancing the material's mechanical strength [43-45]. Alginate forms a hydrogel upon interaction with divalent cations [46]. The adsorption capacity of beads can be increased by adding pore-forming agents like $CaCO_3$ [47-49].

The mixture of alginate and cellulose affects the beads' adsorption capacity [50]. Beads made solely of alginate have a 19% adsorption capacity, which is low compared to those with 10-25% cellulose, showing capacities of 68-80% [51, 52]. Alginate-only beads are less porous and more wrinkled [53, 54].

Research has shown the importance of determining the optimal alginate/cellulose xanthate composition, which is marked by significant swelling power. Viscose solutions were prepared with NaOH concentrations of 4, 6, and 8%. The best formulation was used to make beads with varying alginate to cellulose xanthate ratios (2:0, 2:2, 2:6, 2:16, and 2:30) and the addition of zinc acetate as a crosslinking agent. The functional groups of the extracted cellulose were identified using FTIR. Gravimetric analysis and optical microscopy determined the optimal bead composition based on swelling power. DSC was used to observe thermal characteristics, while SEM-EDX analyzed surface morphology and material properties.

Experimental

Materials and Methds

The bagasse used in this study was obtained from Malang. All chemicals used were of analytical grade and purchased from Merck, including sodium hydroxide (NaOH), hydrochloric acid (HCl), carbon disulfide (CS_2), sodium chlorite ($NaClO_2$), sodium alginate, and zinc acetate.

Extraction of cellulose from bagasse

Bagasse (100 g) was immersed in 2,000 mL of 10% w/w sodium hydroxide (NaOH) at 90 °C for 1 hour. The obtained pulp was rinsed with deionized water several times to wash away the base-soluble structures. The pulp was then treated with 1% w/w sodium chlorite ($NaClO_2$, 200 mL) at pH 5, adjusted with 10% w/w acetic acid at 70 °C for 1 hour, followed by neutralization with deionized water. After that, cellulose was hydrolyzed through reflux with 5% w/w hydrochloric acid (HCl) in a 1:20 solid-to-liquid ratio at 95 °C for 1 hour to remove non-crystalline components, thus separating the dispersed microfibres [55].

Determination of the best NaOH concentration for viscose solution preparation

Cellulose pulp (5 g) was soaked in 40 mL of 20% w/w sodium hydroxide (NaOH) for 3 hours and then stored for ageing at room temperature for 60 hours. Afterwards, the suspension was reacted with 2.5 mL carbon disulfide (CS_2) in a shaker incubator (shaking rate: 150 rpm) at 25 °C for 3 hours to produce cellulose xanthate (T. Wang, Li, and Si 2013). Viscose solution was prepared by dissolving cellulose xanthate into 30 mL of different NaOH concentrations: 4%, 6%, and 8% w/w. Three sets of viscose solution were obtained and labelled CXA-1, CXA-2, and CXA-3. The characteristics of the viscose solution, including density, viscosity, and molecular weight, were determined. Sodium alginate (2 g) was immersed in 50 mL of water and subsequently reacted with acetic acid (CH_3COOH) until thoroughly dissolved. The obtained solution was treated with 2 g of CXA (each of CXA-1, CXA-2, and CXA-3), 2 g calcium carbonate ($CaCO_3$), and deionized water added to make up 100 mL, and then homogenized. The solution was dripped into a 5% zinc acetate solution using a syringe needle and soaked for 24 hours. Thereafter, the obtained beads were neutralized with deionized water. Removal of $CaCO_3$ granules from the beads was carried out by reacting the beads with a diluted acidic solution. One volume of the cross-linked beads was mixed with eight volumes of hydrochloric acid

(HCl, 1 mmol/L) in a flask and then placed in a shaker incubator at 150 rpm until no bubbles were observed. The attained beads were rinsed to a neutral pH with deionized water [55].

Three sets of beads were obtained and labelled as CXA-1, CXA-2, and CXA-3. The best NaOH concentration for viscose solution preparation was determined based on the density, viscosity, and molecular weight of the solution and the swelling power of the produced beads.

Preparation of beads with various compositions of alginate:cellulose xanthate

Cellulose xanthate with the best properties was utilized to determine the optimal composition ratio of alginate to cellulose xanthate for bead synthesis. The compositions evaluated were 2:0, 2:2, 2:6, 2:16, and 2:30.

Density, viscosity, and molecular weight

Density of the viscose solution is defined by the following equation, where d is the density, m is the mass, and v is the volume.

$$d = \frac{m}{v} \quad (1)$$

While viscosity of the viscose solution is defined by Equation (2).

$$\frac{\eta_0}{\eta_1} = \frac{d_0 t_0}{d_0 t_1} \quad (2)$$

Where, η_0 is water viscosity, η_1 is the viscosity of solution, t_0 is the time it takes for the water to flow through the capillary pipe, and t_1 is the time it takes for the solution to flow through the capillary tube.

Molecular weight of the viscose solution is calculated with Euqations (3) and (4).

$$\eta* = \frac{t*}{t \times \eta} \quad (3)$$

$$\eta_{sps} = \frac{(\eta - \eta*)}{\eta*} \quad (4)$$

$$\eta_{int} = \frac{\eta_{sps}}{c} \quad (5)$$

$$\eta_{int} = KM^a \quad (6)$$

In which, η* is solvent viscosity (Pa.s), t* is solvent flow time (s), η is viscosity of the solution, t is solvent flow time (s), η_{sps} is specific viscosity, η_{int} is intrinsic viscosity, c is solvent concentration, K, α is Mark-Houwink constants ($K = 9.8 \times 10^{-3}$ and $\alpha = 0.9$), and M is the molecular weight.

Beads swelling

Swelling ratio is determined by immersing 0.5 g sample in excess deionized water at 20 ˚C. The swelling ratio of the beads is defined by Equation (7).

$$\text{Swelling ratio} \frac{(W_t - W_0)}{W_0} \times 100\% \quad (7)$$

Where, $W_。$ and Wt is the mass of the dry and swollen beads, respectively, at a time (t).

FTIR-spectra analysis

FTIR analysis was performed using a Bruker Alpha instrument. A 5 mg sample was pressed into a disk for measurement.

DSC-thermal analysis

Several milligrams of the sample were placed in a crucible and then positioned inside a DSC furnace. Measurements were conducted over a temperature range of 30-400 °C at a heating rate of 10 °C/min.

Optical microscope-shape and diameter analysis

The shape and diameter of the beads formed of alginate:cellulose xanthate were observed using optical microscope at 0.75 mm magnification and the results were analyzed with ImageJ software.

Characterization of surface morphology with SEM-EDX

Surface morphology was characterized using SEM-EDX at magnifications of 500x and 15,000x.

Results and discussion

In this study, the production of alginate-cellulose xanthate beads resulted in structures with enhanced rigidity. This effect is attributed to the cross-linking agent that fortifies the bead's outer layer. Specifically, cross-linkages form between the alginate's negatively charged carboxylate groups (-COO-) and divalent zinc ions (Zn^{2+}). In addition, the cellulose xanthate incorporated into the alginate solution interacts and reacts with zinc ions, as supported by the literature [56]. Moreover, hydrogen bonding between cellulose xanthate molecules contributes to the stability of the beads. Figure 1 depicts the physical appearances of the beads in both wet and dry states.

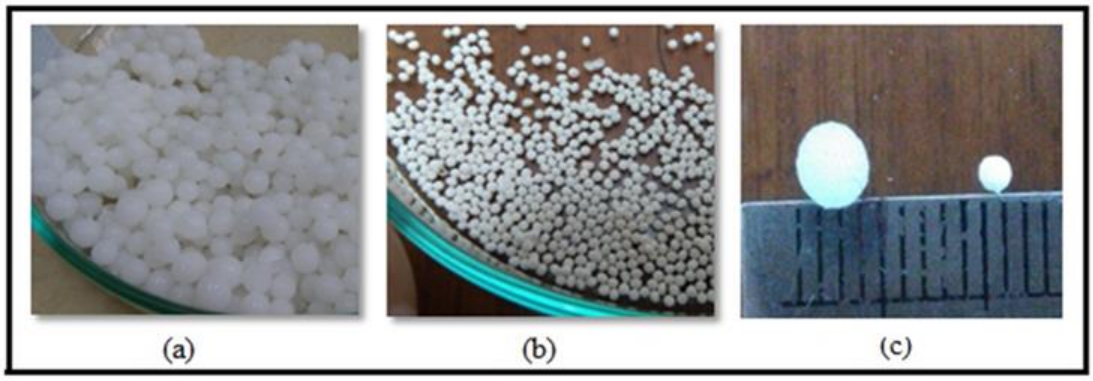

Figure 1. a) Wet beads, b) dry beads, and c) comparison of diameters for wet and dry beads

Table 1. Density, Viscosity, Molecular Weight (MW), and Swelling Ratio (SR) of the beads fabricated of viscose cellulose solution prepared with various NaOH Concentrations

Sample	Density (gr/mL)	Viscosity (Pa.s)	MW
Deionized Water	0.997	0.0009	-
CXA-1	1.071	0.006	70.460
CXA-2	1.099		171.686
CxA-3	1.085	0.008	22.942

Varying the NaOH concentration has clearly affected the physical properties of the viscose solution, including density, viscosity, and molecular weight. The detailed result presented in Table 1 shows that the beads obtained from 6% NaOH variation has predominantly surpassed the products of other variations on all parameters.

This concentration was used in the preparation of viscose solution CXA-2, producing solution of 1,099 gr/ml density and viscosity of 0.024 Pa.s. The viscosity of cellulose solution prepared using 6% NaOH ranges from 2.3-2.5 Pa.s [57].

This huge difference in result occurred because the cellulose employed in this study

was of natural material, while his research used synthetic cellulose. CX2 also exhibits higher molecular weight compared to the product of other variations, thus was selected for further use as the precursor in beads production.

Varying the concentration of NaOH used to dissolve cellulose xanthate suspension apparently has affected the swelling ratio of the produced beads as well. Table 1 and Figure 2 show that the utilization of 6% (w/w) NaOH (CXA-2) resulted in the best viscose solution.

High swelling ratio is one of the reasons CXA-2 was chosen for further use as the precursor for beads production. This result is supported by FTIR spectra of CXA-2 (Figure 3) which shows that it has the highest intensity of OH group among all samples, indicating the abundance of OH group contained within the beads. The abundant OH groups within alginate and cellulose xanthate beads bind water molecules and lead to an increase in swelling ratio.

We compared alginate:cellulose xanthate composites ranging from a 2:0 to a 2:30 ratio, incrementally increasing the cellulose content during bead fabrication. An increase in cellulose xanthate composition leads to a more substantial water-binding capacity between the molecule and the crosslinking agent, observable during the immersion process. Consequently, the beads with 2:16 and 2:30 ratios are larger than those of other composites, as illustrated in Figure 4.

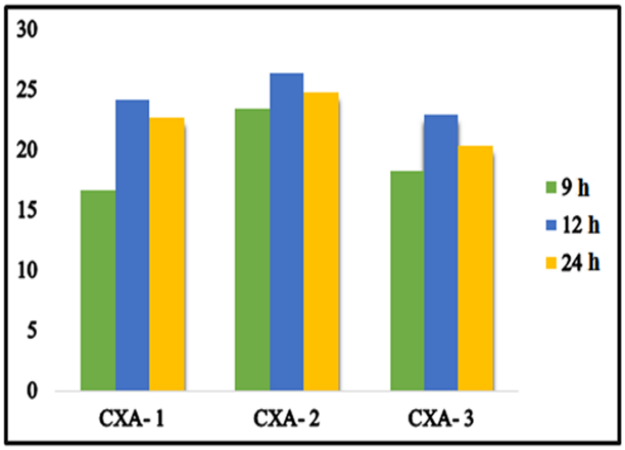

Figure 2. Swelling ratio of beads prepared with viscose solutions varying in NaOH concentration

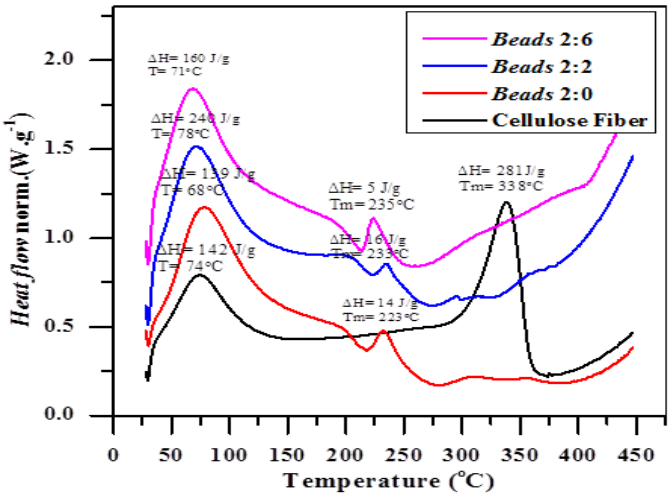

Figure 3. Thermogram of cellulose fibre and beads of various alginate/cellulose xanthate compositions of 2:0, 2:2, and 2:6

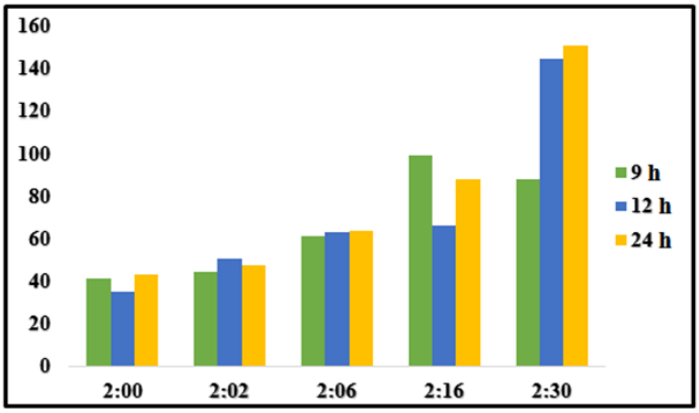

Figure 4. Swelling ratio of beads prepared with various alginate/cellulose xanthate compositions

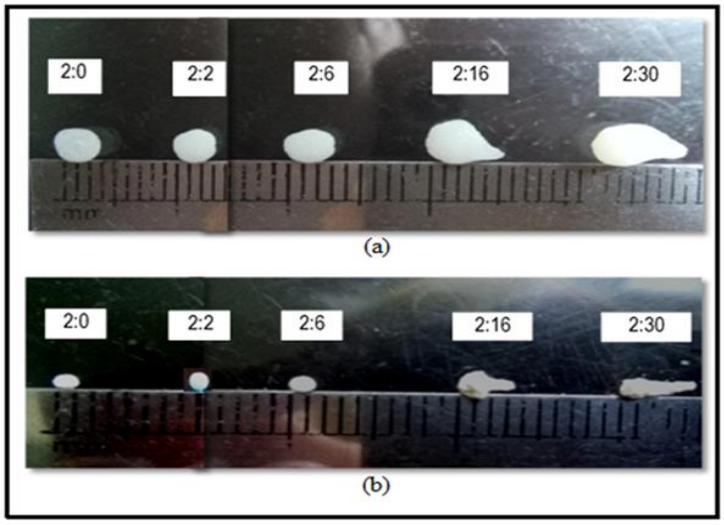

Figure 5. Physical appearance of (a) wet, and (b) dry beads of various alginate/cellulose xanthate compositions

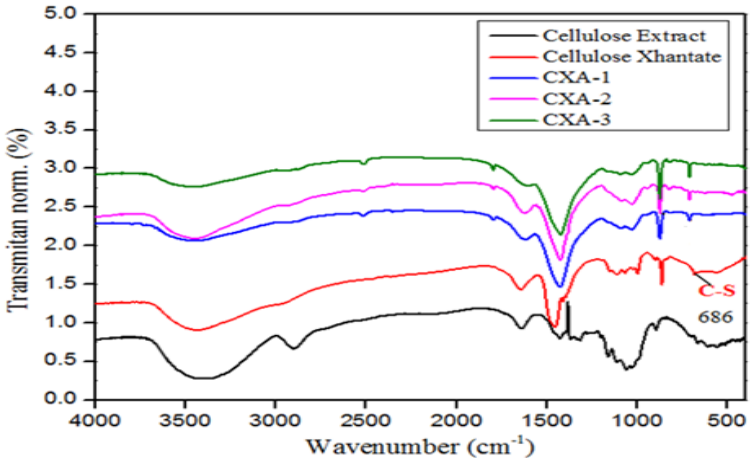

Figure 6. FTIR spectra of cellulose extract, cellulose xanthate, CXA-1, CXA-2, and CXA-3 beads

The profusion of hydroxyl (-OH) groups within these composites also contributes to an increase in swelling power. However, higher levels of cellulose xanthate present challenges in forming perfectly spherical beads. Although a high content of hydroxyl groups in the beads correlates with increased swelling power, the FTIR spectra show that beads with a 2:6 ratio are less crystalline than those with a 2:2 ratio; the latter exhibits a sharper hydroxyl peak (Figure 6). This sharper peak indicates that the 2:2 ratio beads have higher crystallinity and density compared to the 2:6 ratio beads. The DSC measurements, presented in Figure 7, support this finding; as the enthalpy of fusion (ΔHf) value increases, so does the material crystallinity, which facilitates bead formation. In this study, beads with a 2:2 ratio displayed the highest ΔHf value of 16 J/g, confirming their superior crystallinity among the samples tested.

The study revealed that the alginate to cellulose xanthate ratio is a crucial factor in determining the geometry of the beads. Beads with a 2:0 ratio exhibit a more uniform shape compared to the 2:2 ratio, and those with a 2:6 ratio tend to have creased surfaces.

Diameter analysis, conducted using ImageJ software, indicates significant size differences among the beads. Figure 8 delineates the diameter of swollen beads after a 24-hour period, highlighting that beads with a 2:6 alginate/cellulose xanthate ratio have the largest average diameter, measuring up to 2.1 mm. It is evident that an increased cellulose ratio directly correlates with bead size.

The SEM images, as depicted in Figure 7, reveal that adding cellulose significantly alters the bead surface. Even at 500x magnification, the impact is visible as cellulose microfibrils create a more porous surface, which becomes increasingly evident at 15,000x. A higher concentration of cellulose in the beads leads to the formation of pores across the entire bead surface. In contrast, the 2:0 ratio beads, made solely of alginate, present a smoother and poreless exterior. Furthermore, the 2:6 ratio beads exhibit deeper and more extensive cavities compared to the 2:2 ratio, corroborating the optical microscopy findings (Figure 5), which show that the 2:6 beads have a heavily creased surface and are not as spherical as the 2:2 beads.

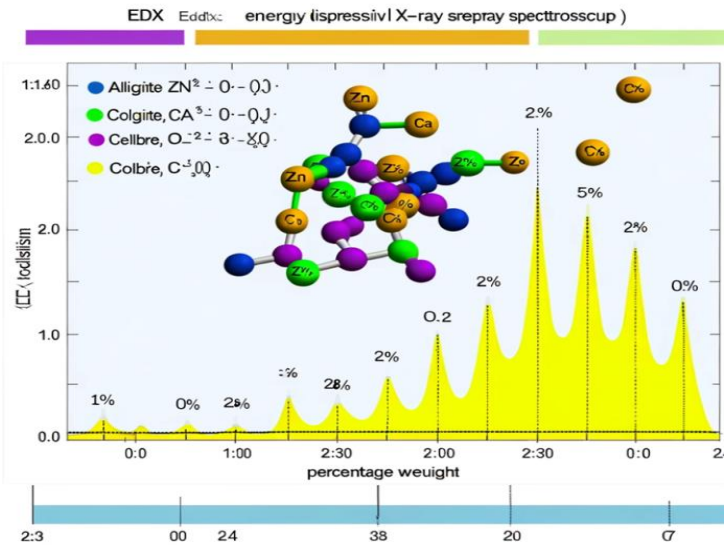

Figure 7. Image representing the EDX analysis data from Table 2 in the paper, showcasing the percentage weight of elements (Zn, Ca, O, C) in alginate/cellulose beads at different ratios

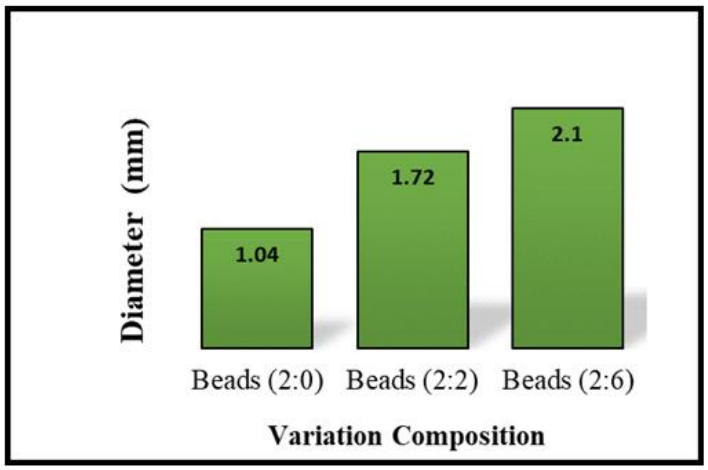

Figure 8. Diameter of swollen beads with various alginate/cellulose xanthate compositions: 2:0, 2:2, and 2:6

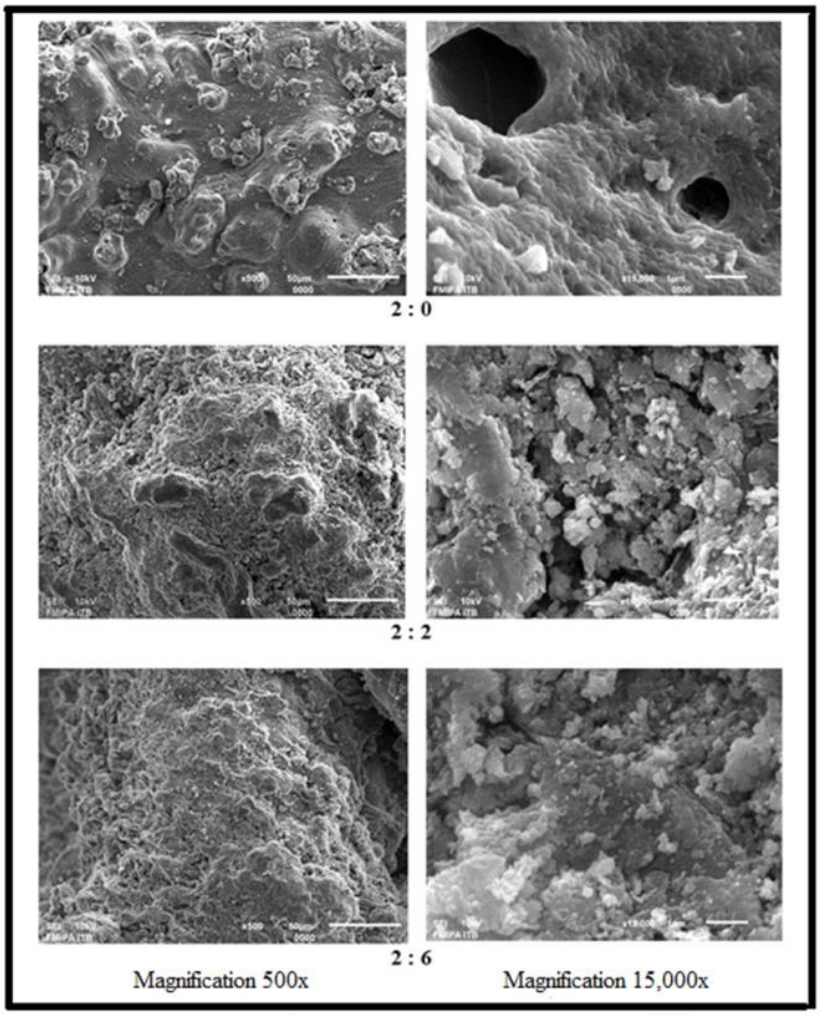

Figure 9. SEM images of alginate/cellulose xanthate composites at 500x and 15,000x magnifications, featuring composition variations of 2:0, 2:2, and 2:6

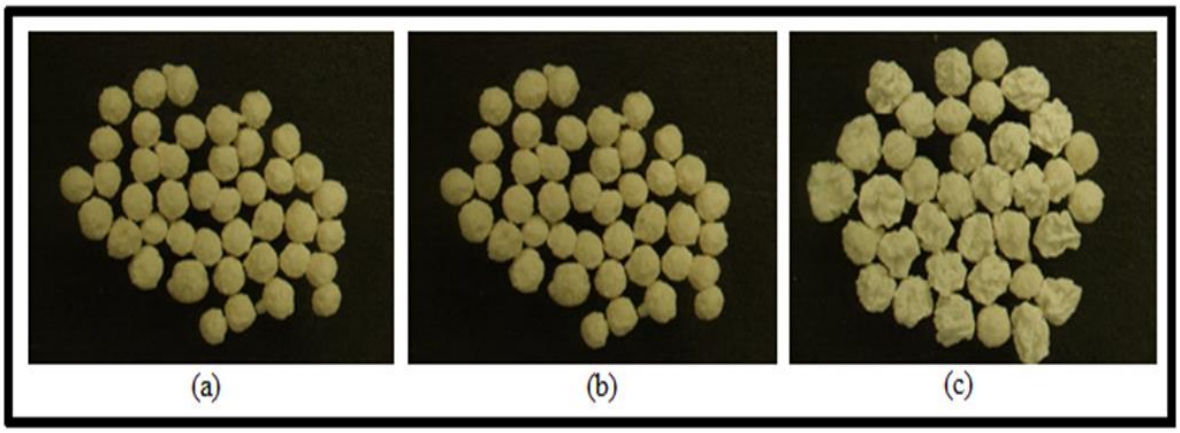

Figure 10. Optical microscopic images of beads with varying alginate/cellulose xanthate compositions: (a) 2:0, (b) 2:2, and (c) 2:6

Table 2 presents the SEM-EDX data, which clearly shows an increase in Zn ion percentage with a higher cellulose ratio, highlighting the strong binding affinity between Zn^{2+} ions and the active groups in cellulose. This is supported by the FTIR spectra (Figure 6), which demonstrate significant alterations in the alginate spectra, especially in the 89-1200 cm^{-1} region, reflecting the bond vibrations related to β-glycosidic linkages, C-O and OH in-plane bending, C–O–C anti-symmetric bridge stretching, and C–O stretching [73]. Table 2 summarizes the SEM-EDX data for alginate/cellulose beads with different alginate to cellulose ratios, specifically 2:0, 2:2, and 2:6. The SEM-EDX data provides insight into the elemental composition of the beads, showing the weight percentages of zinc (Zn), calcium (Ca), oxygen (O), and carbon (C) in each type of bead.

As the cellulose ratio increases, there is a noticeable rise in the percentage of Zn ions, signifying a strong interaction between Zn^{2+} ions and the active groups in cellulose, which points to an affinity for Zn^{2+} within the cellulose structure. This observation is further substantiated by alterations in the FTIR spectra, especially in the 890-1200 cm^{-1} region, which reflects the bond vibrations related to β-glycosidic linkages C-O and OH in-plane bending, C–O–C anti-symmetric bridge stretching, and C–O stretching.

The SEM-EDX analysis depicted in the image provided visually represents this data. The peaks correspond to the elemental composition, and their heights reflect the weight percentages, as detailed in Table 2.

The graph is a representation of the elemental analysis, where the vertical axis indicates the weight percentage and the horizontal axis represents the detected elements. The increase in the peak corresponding to Zn with higher ratios of cellulose is clearly illustrated, which aligns with the table's data, highlighting the beads' changing composition with varying ratios of alginate to cellulose.

Figure 10 shows the DSC thermograms of cellulose fibers and beads with varying alginate/cellulose xanthate ratios. These thermograms indicate that an increased cellulose content within the beads corresponds to a more amorphous structure. Notably, beads with ratios of 2:16 and 2:30 exhibit a very low enthalpy of fusion (ΔHf), indicative of an amorphous structure, which results in a higher swelling ratio and presents challenges in maintaining spherical shapes, as presented in

Figure 4. Furthermore, the data suggest a proportional relationship between the cellulose ratio and the melting point of the material. This increase in melting point, as seen in the thermograms, can be attributed to the rise in molecular weight, which is reflective of the interactions within the polymer matrices, the influence of particle size, and the homogeneity of the particles.

Figure 6 displays the FTIR spectra for CX-1, CX-2, and CX-3 beads, alongside those for cellulose extract and cellulose xanthate. We observed the stretching of the OH group at 3441 cm^{-1}, the aliphatic C-H bond vibration at 2930 cm^{-1}, the C-C bond at 1616-1427 cm^{-1}, and the C-O-C bond at 1093-1031 cm^{-1}. The spectra reveal that extraction significantly alters the material, showcasing a clear distinction in functional groups between the cellulose extract and cellulose xanthate. Notably, the cellulose extract spectra lack several peaks, including the one at 1732 cm^{-1}, which we attribute to the acetyl (CH3OC-) group vibration, the aromatic C=C group at 1515 cm^{-1}, and a peak at 830 cm^{-1}. These absences indicate the removal of lignin compounds during extraction, aligning with findings by [65]. Furthermore, the increase in cellulose content in the extract is evidenced by the enhanced peak intensity at 1162-1034 cm^{-1}, corresponding to the C-O-C group vibration of the pyranose ring, and at 896 cm^{-1}, indicative of the β-glycosidic bond in cellulose, mirroring results reported by [73].

In addition, Figure 6 illustrates that CX-A1, CX-A2, and CX-A3 show varying intensities of the –OH group peak. This variation suggests that higher concentrations of sodium hydroxide (NaOH) in the viscose solution preparation lead to more cellulose being extracted, as indicated by the presence of a sharper –OH group peak. This trend persists until reaching an optimum concentration, beyond which the extracted cellulose content begins to diminish with further increases in NaOH concentration.

Figure 11 demonstrates that altering the alginate/cellulose xanthate composition noticeably impacts the FTIR spectra, particularly the OH group peak intensity. In beads with a 2:0 alginate-to-cellulose xanthate ratio, we observe a weak absorption of the OH group at 3441 cm^{-1}, which sharply increases in the 2:2 and 2:6 ratio products. The spectral patterns of the materials before (cellulose xanthate) and after ionic gelation with Zn^{2+} ions (beads with 2:0, 2:2, and 2:6 ratios) highlight the effective crosslinking between Zn^{2+} ions and cellulose polymers. The binding region for Zn^{2+} ions is characterized by β-glycoside bond vibration, C-O, OH in-plane bending, C-O-C anti-symmetric bridge stretching, and C-O stretching, corroborating the findings of [65].

The structural analysis of cellulose and cellulose xanthate in 11 reveals significant insights into their molecular architecture and interaction dynamics. The process of extracting and modifying cellulose from bagasse into cellulose xanthate significantly changes its chemical structure, increasing its application in forming alginate-cellulose xanthate granules. The FTIR spectrum highlighted in the image shows transformations characterized by the appearance and change of functional groups, indicating successful xanthation. This structural reconfiguration results in an increased abundance of hydroxyl groups, facilitating enhanced water absorption and swelling behavior, which is important for the beads application in adsorption and encapsulation. The interaction between alginate and cellulose xanthate, mediated by cross-linking agents, further contributes to the mechanical stability and porosity of the beads, thereby optimizing their function in various environmental and biomedical applications. This analysis underscores the importance of molecular

structure in determining material properties and performance, offering a pathway for the synthesis of tailored biopolymer composites with desired characteristics. Figure 10 provides FTIR spectra for cellulose extract and cellulose xanthate, which are compared to the spectra of CX-1, CX-2, and CX-3 beads. The FTIR analysis reveals distinct features such as the stretching of the OH group at 3441 cm^{-1}, the aliphatic C-H bond vibration at 2930 cm^{-1}, the C-C bond at 1616-1427 cm^{-1}, and the C-O-C bond at 1093-1031 cm^{-1}. These observations indicate significant alterations in the material upon extraction, resulting in a clear distinction in functional groups between the cellulose extract and cellulose xanthate.

The cellulose extract spectra are characterized by the absence of several peaks present in the cellulose xanthate spectra. These absent peaks include the one at 1732 cm^{-1}, attributed to the acetyl (CH_3OC-) group vibration, the aromatic C=C group at 1515 cm^{-1}, and a peak at 830 cm^{-1}, indicating the removal of lignin compounds during the extraction process. The increase in cellulose content in the extract is evidenced by the enhanced peak intensity at 1162-1034 cm^{-1}, corresponding to the C-O-C group vibration of the pyranose ring, and at 896 cm^{-1}, indicative of the β-glycosidic bond in cellulose. Furthermore, the intensity variations of the –OH group peak in the spectra of CX-A1, CX-A2, and CX-A3 suggest that higher concentrations of sodium hydroxide (NaOH) in the viscose solution preparation lead to more cellulose being extracted, as indicated by a sharper –OH group peak.

Table 2. SEM-EDX result of alginate/cellulose beads

Alginate: Cellulose Ratio	Percent Weight of Each Element			
	Zn	Ca	O	C
2:0	7.67 %	5.08 %	4.40 %	43.44%
2:2	24.10 %	2.46 %	39.18 %	33.74 %
2:6	33.14 %	1.79 %	37.16 %	27.25 %

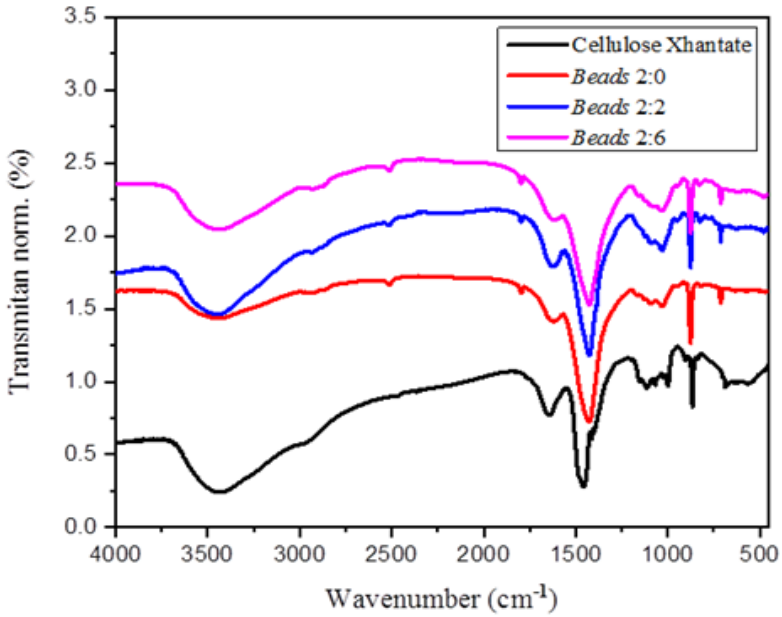

Figure 11. FTIR spectra of cellulose xanthate and beads of 2:0, 2:2, and 2:6 composition ratio

This FTIR spectral analysis is crucial for understanding the structural changes and the nature of interactions within the beads, which are influenced by the processing conditions and the materials used. The molecular structure determined by FTIR plays a significant role in the material properties and performance, especially for applications that require specific interactions, like adsorption and encapsulation in environmental and biomedical fields.

Conclusion

This study demonstrates that a 6% sodium hydroxide (NaOH) concentration yields the optimal results for preparing cellulose viscose solutions used in synthesizing alginate/cellulose xanthate beads. We arrived at this conclusion by comparing the swelling ratios of products produced under various conditions. The optimal concentration variation is characterized by the highest swelling ratio, recorded at 50.8%, and the most pronounced intensity of the OH group in the infrared (IR) spectra. Moreover, the ideal alginate/cellulose xanthate composition is achieved at a 2:2 ratio, where the beads showcase the most significant intensity of the OH group on FTIR spectra, a heat flow (ΔHf) value of 16 J/g, and a swelling ratio of approximately 63.8%. Characterization outcomes indicate that incorporating cellulose in varied compositions markedly influences the beads' shape, porosity, crystallinity, swelling ratio, diameter, and surface topology. Furthermore, the findings suggest that increasing the polymer composition leads to a higher formation of pores, thereby enhancing the swelling capability and diameter of the beads.

Disclosure Statement

No potential conflict of interest was reported by the authors.

Funding

This research did not receive any specific grant from funding agencies in the public, commercial, or not-for-profit sectors.

Authors' Contributions

All authors contributed to data analysis, drafting, and revising of the paper and agreed to be responsible for all the aspects of this work.

Orcid

Eny Yulianti
https://orcid.org/0000-0002-4182-7720
Lilik Miftahul Khoiroh
https://orcid.org/0000-0001-6634-6571
Rif'atul Mahmudah
https://orcid.org/0009-0004-3090-1501
Sindi Puspitasari
https://orcid.org/0009-0002-0580-2697
Faiqotul Himmah
https://orcid.org/0009-0001-3737-7616
Tzu-Teng Huang
https://orcid.org/0009-0009-2014-6596
Imtiaz Ali Laghari
https://orcid.org/0000-0001-5091-0297
Ahmad Zikri
https://orcid.org/0000-0002-6933-7379
Mohammad Abdullah
https://orcid.org/0000-0003-1775-7926
Rahadian Zainul
https://orcid.org/0000-0002-3740-3597
Tarek A. Elkhooly
https://orcid.org/0000-0002-9278-0977

References

[1]. Quereshi S., Naiya T.K., Mandal A., Dutta S. Residual sugarcane bagasse conversion in India: current status, technologies, and policies, *Biomass Conversion and Biorefinery*, 2022, **12**:3687 [Crossref], [Google Scholar], [Publisher]

[2]. Hasanudin H., Asri W.R., Zulaikha I.S., Ayu C., Rachmat A., Riyanti F., Hadiah F., Zainul R., Maryana R. Hydrocracking of crude palm oil to a

biofuel using zirconium nitride and zirconium phosphide-modified bentonite, *RSC advances*, 2022, **12**:21916 [Crossref], [Google Scholar], [Publisher]

[3]. Zainul R., Oktavia B., Dewata I., Efendi J. *IOP Conference Series: Materials Science and Engineering*, 2018, **335**:012039 [Crossref], [Google Scholar], [Publisher]

[4]. Zainul R. Design and modification of copper oxide electrodes for improving conversion coefficient indoors lights (PV-Cell) photocells, *Der Pharma Chemica*, 2016, **8**:338 [Google Scholar], [Publisher]

[5]. Zhou X., Hao Y., Zhang X., He X., Zhang C. Cellulose-based polymers, *Physical Sciences Reviews*, 2023, **8**:2001 [Crossref], [Google Scholar], [Publisher]

[6]. Putri G.E., Gusti F.R., Sary A.N., Zainul R. *Journal of Physics: Conference Series*, 2019, **1317**:012027 [Crossref], [Google Scholar], [Publisher]

[7]. Zainul R. Effect of Temperature and Particle Motion against the ability of ZnO Semiconductor Photocatalyst in Humic Acid, *Der Pharmacia Lettre*, 2016, **15**:120 [Google Scholar], [Publisher]

[8]. Sharif S.N.M., Hashim N., Isa I.M., Bakar S.A., Saidin M.I., Ahmad M.S., Mamat M., Hussein M.Z., Zainul R., Kamari A. The effect of swellable carboxymethyl cellulose coating on the physicochemical stability and release profile of a zinc hydroxide nitrate–sodium dodecylsulphate–imidacloprid, *Chemical Physics Impact*, 2021, **2**:100017 [Crossref], [Google Scholar], [Publisher]

[9]. Kayan G.Ö., Kayan A. Composite of natural polymers and their adsorbent properties on the dyes and heavy metal ions, *Journal of Polymers and the Environment*, 2021, **29**:3477 [Crossref], [Google Scholar], [Publisher]

[10]. Muthukumaran P., Suresh Babu P., Karthikeyan S., Kamaraj M., Aravind J. Tailored natural polymers: a useful eco-friendly sustainable tool for the mitigation of emerging pollutants: a review, *International Journal of Environmental Science and Technology*, 2021, **18**:2491 [Crossref], [Google Scholar], [Publisher]

[12]. Abdelhamid H.N., Mathew A.P. Cellulose-based materials for water remediation: adsorption, catalysis, and antifouling, *Frontiers in Chemical Engineering*, 2021, **3**:790314 [Crossref], [Google Scholar], [Publisher]

[13]. Zainul R., Abd Azis N., Md Isa I., Hashim N., Ahmad M.S., Saidin M.I., Mukdasai S., Zinc/aluminium–quinclorac layered nanocomposite modified multi-walled carbon nanotube paste electrode for electrochemical determination of bisphenol A, *Sensors*, 2019, **19**:941 [Crossref], [Google Scholar], [Publisher]

[14]. Tamarani A., Zainul R., Dewata I. Preparation and characterization of XRD nano Cu-TiO2 using sol-gel method. *Journal of Physics: Conference Series*, 2019, **1185**:012020 [Crossref], [Google Scholar], [Publisher]

[15]. Sjahro N., Yunus R., Abdullah L.C., Rashid S.A., Asis A.J., Akhlisah Z. Recent advances in the application of cellulose derivatives for removal of contaminants from aquatic environments, *Cellulose*, 2021, **28**:7521 [Crossref], [Google Scholar], [Publisher]

[16]. Aziz T., Farid A., Haq F., Kiran M., Ullah A., Zhang K., Li C., Ghazanfar S., Sun H., Ullah R. A review on the modification of cellulose and its applications, *Polymers*, 2022, **14**:3206 [Crossref], [Google Scholar], [Publisher]

[17]. Li X., Wan C., Tao T., Chai H., Huang Q., Chai Y., Wu Y. An overview of the development status and applications of cellulose-based functional materials. *Cellulose*, 2024, **31**:61 [Crossref], [Google Scholar], [Publisher]

[18]. Zainul R., Isa I.M., Yazid A.M., Nur S., Hashim N., Mohd Sharif S.N., Saidin M.I., Ahmad M.S., Suyanta M.S., Amir Y. Enhanced electrochemical sensor for electrocatalytic glucose analysis in orange juices and milk by the

integration of the electron-withdrawing substituents on graphene/glassy carbon electrode, *Journal of Analytical Methods in Chemistry*, 2022, **2022** [Crossref], [Google Scholar], [Publisher]

[19]. Abd Azis N., Isa I.M., Hashim N., Ahmad M.S., Yazid S.N.A.M., Saidin M.I., Si S.M., Zainul R., Ulianas A., Mawardi M. Synergistic effect of zinc/aluminium-layered double hydroxide-clopyralid carbon nanotubes paste electrode in the electrochemical response of dopamine, acetaminophen, and bisphenol A, *International Journal of Electrochemical Science*, 2020, **15**:9088 [Crossref], [Google Scholar], [Publisher]

[20]. Mohd Yazid S.N.A., Md Isa I., Ali N.M., Hashim N., Saidin M.I., Ahmad M.S., Asiri A.M., Khan A., Zainul R. Graphene/iridium (III) dimer complex composite modified glassy carbon electrode as selective electrochemical sensor for determination of hydroquinone in real-life water samples, *International Journal of Environmental Analytical Chemistry*, 2022, **102**:2607 [Crossref], [Google Scholar], [Publisher]

[21]. Rais N.S.M., Isa I.M., Hashim N., Saidin M.I., Yazid S.N.A.M., Ahmad M.S., Zainul R., Mukdasai S. Simultaneously determination of bisphenol A and uric acid by zinc/aluminum-layered double hydroxide-2-(2, 4-dichlorophenoxy) propionate paste electrode, *International Journal of Electrochemical Science*, 2019, **14**:7911 [Crossref], [Google Scholar], [Publisher]

[22]. Zainul R., Hashim N., Yazid S.N.A.M., Sharif S.N.M., Ahmad M.S., Saidin M.I., Sobry M., Isa I.M. Magnesium layered hydroxide-3-(4-methoxyphenyl) propionate modified single-walled carbon nanotubes as sensor for simultaneous determination of Bisphenol A and Uric Acid, *International Journal of Electrochemical Science*, 2021, **16**:210941 [Crossref], [Google Scholar], [Publisher]

[23]. Vikulina A.S., Campbell J. Biopolymer-Based Multilayer Capsules and Beads Made via Templating: Advantages, Hurdles and Perspectives, *Nanomaterials*, 2021, **11**:2502 [Crossref], [Google Scholar], [Publisher]

[24]. Khandbahale S.V. Microencapsulation-A novel approach in drug delivery: a review, *Asian Journal of Research in Pharmaceutical Science*, 2020, **10**:39 [Crossref], [Google Scholar], [Publisher]

[25]. Abd Azis N., Isa I.M., Hashim N., Ahmad M.S., Yazid S.N.A.M., Saidin M.I., Si S.M., Zainul R., Ulianas A., Mukdasai S. Voltammetric determination of bisphenol a in the presence of uric acid using a zn/al-ldh-qm modified MWCNT paste electrode, *International Journal of Electrochemical Science*, 2019, **14**:10607 [Crossref], [Google Scholar], [Publisher]

[26]. Hasanudin H., Asri W.R., Zulaikha I.S., Ayu C., Rachmat A., Riyanti F., Hadiah F., Zainul R., Maryana R. Hydrocracking of crude palm oil to a biofuel using zirconium nitride and zirconium phosphide-modified bentonite, *RSC advances*, 2022, **12**:21916 [Crossref], [Google Scholar], [Publisher]

[27]. Nikonam M R., Pugh M.D., Drew R.A. Pore structure, porosity and compressive strength of highly porous reaction-bonded silicon nitride ceramics with various grain morphologies, *Journal of materials science*, 2020, **55**:509 [Crossref], [Google Scholar], [Publisher]

[28]. Qiao L., Li S., Du K. Fabrication and characterization of porous cellulose beads with high strength and specific surface area via preliminary chemical cross-linking reaction for protein separation, *Biochemical Engineering Journal*, 2020, **153**:107412 [Crossref], [Google Scholar], [Publisher]

[29]. Tajudin M.H.A., Ahmad M.S., Isa I.M., Hashim N., Ul-Hamid A., Saidin M.I., Zainul R., Si S.M. Sensitive determination of uric acid at layered zinc hydroxide-sodium dodecyl sulphate-propoxur nanocomposite, *Journal of*

Electrochemical Science and Engineering, 2022, **12**:331 [Google Scholar], [Publisher]
[30]. Rahmawati F., Heliani K.R., Wijayanta A.T., Zainul R., Wijaya K., Miyazaki T., Miyawaki J. Alkaline leaching-carbon from sugarcane solid waste for screen-printed carbon electrode, *Chemical Papers*, 2023, **77**:3399 [Crossref], [Google Scholar], [Publisher]
[31]. Biswas S.,Pal, A., Application of biopolymers as a new age sustainable material for surfactant adsorption: A brief review, *Carbohydrate Polymer Technologies and Applications*, 2021, **2**:100145 [Crossref], [Google Scholar], [Publisher]
[32]. Rahmadiawan D., Abral H., Ilham M.K., Puspitasari P., Nabawi R.A., Shi S.C., Sugiarti E., Muslimin A.N., Chandra D., Ilyas R. Enhanced UV blocking, tensile and thermal properties of bendable TEMPO-oxidized bacterial cellulose powder-based films immersed in PVA/Uncaria gambir/ZnO solution, *Journal of materials research and technology*, 2023, **26**:5566 [Crossref], [Google Scholar], [Publisher]
[33]. Putri G.E., Gusti F.R., Sary A.N., Zainul R. Synthesis of silver nanoparticles used chemical reduction method by glucose as reducing agent, *Journal of Physics: Conference Series*, 2019, **1317**:012027 [Crossref], [Google Scholar], [Publisher]
[34]. Zainul R., Oktavia B., Dewata I., Efendi J. Study of Internal Morphology on Preparation of Cu2OThin-Plate using Thermal Oxidation, *Journal of Physics: Conference Series*, 2018, **1116**:042046 [Crossref], [Google Scholar], [Publisher]
[35]. Mokhtari A., Sabzi M., Azimi H. 3D porous bioadsorbents based on chitosan/alginate/cellulose nanofibers as efficient and recyclable adsorbents of anionic dye, *Carbohydrate polymers*, 2021, **265**:118075 [Crossref], [Google Scholar], [Publisher]
[36]. Mohd Sharif S.N., Hashim N., Md Isa I., Abu Bakar S., Idris Saidin M., Syahrizal Ahmad M., Mamat M., Zobir Hussein M., Zainul R. Carboxymethyl cellulose hydrogel based formulations of zinc hydroxide nitrate-sodium dodecylsulphate-bispyribac nanocomposite: Advancements in controlled release formulation of herbicide, *Journal of nanoscience and nanotechnology*, 2021, **21**:5867 [Crossref], [Google Scholar], [Publisher]
[37]. Sharif S.N., Hashim N., Isa I.M., Bakar S.A., Saidin M.I., Ahmad M.S., Mamat M., Hussein M.Z., Zainul R., Chitosan as a coating material in enhancing the controlled release behaviour of zinc hydroxide nitrate–sodium dodecylsulphate–bispyribac nanocomposite, *Chemical Papers*, 2021, **75**:611 [Crossref], [Google Scholar], [Publisher]
[38]. Alkhatib H., Assadpour E., Sabere A.S.M., Mohamed F., Jafari S.M. Optimizing the encapsulation of black seed oil into alginate beads by ionic gelation, *Journal of food engineering*, 2022, **328**:111065 [Crossref], [Google Scholar], [Publisher]
[39]. Naranjo-Durán A.M., Quintero-Quiroz J., Rojas-Camargo J., Ciro-Gómez G.L. Modified-release of encapsulated bioactive compounds from annatto seeds produced by optimized ionic gelation techniques, *Scientific Reports*, 2021, **11**:1317 [Crossref], [Google Scholar], [Publisher]
[41]. Jeong C., Kim, S., Lee, C., Cho, S.,Kim, S.-B., Changes in the physical properties of calcium alginate gel beads under a wide range of gelation temperature conditions, *Foods*, 2020, **9**:180 [Crossref], [Google Scholar], [Publisher]
[42]. Reurink D., Willott, J., Roesink, H.,De Vos, W., Role of polycation and cross-linking in polyelectrolyte multilayer membranes, *ACS Applied Polymer Materials*, 2020, **2**:5278 [Crossref], [Google Scholar], [Publisher]
[43]. Schirmer U., Ludolph, J., Rothe, H., Hauptmann, N., Behrens, C., Bittrich, E., Schliephake, H.,Liefeith, K., Tailored Polyelectrolyte Multilayer Systems by Variation

of Polyelectrolyte Composition and EDC/NHS Cross-Linking: Physicochemical Characterization and In Vitro Evaluation, *Nanomaterials*, 2022, **12**:2054 [Crossref], [Google Scholar], [Publisher]
[44]. Self J., Hahn, N.T., Fong, K.D., McClary, S.A., Zavadil, K.R.,Persson, K.A., Ion pairing and redissociaton in low-permittivity electrolytes for multivalent battery applications, *The journal of physical chemistry letters*, 2020, **11**:2046 [Crossref], [Google Scholar], [Publisher]
[45]. Baskin A.,Prendergast, D., Ion solvation engineering: how to manipulate the multiplicity of the coordination environment of multivalent ions, *The journal of physical chemistry letters*, 2020, **11**:9336 [Crossref], [Google Scholar], [Publisher]
[46]. Makarova A.O., Derkach S.R., Khair T., Kazantseva M.A., Zuev Y.F., Zueva O.S. Ion-induced polysaccharide gelation: Peculiarities of alginate egg-box association with different divalent cations, *Polymers*, 2023, **15**:1243 [Crossref], [Google Scholar], [Publisher]
[47]. Roquero D.M., Othman A., Melman A., Katz E. Iron (III)-cross-linked alginate hydrogels: A critical review, *Materials Advances*, 2022, **3**:1849 [Crossref], [Google Scholar], [Publisher]
[48]. Zhang W., Ou J., Tang M., He Q., Long A., Luo S., Sun S., Wan J., Gao Y., Zhou L. Physically-crosslinked activated CaCO3/polyaniline-polypyrrole-modified GO/alginate hydrogel sorbent with highly efficient removal of copper (II) from aqueous solution, *Chemical Engineering Journal*, 2022, **431**:133375 [Crossref], [Google Scholar], [Publisher]
[49]. Wang L., Wang J.,Wei Y. Facile synthesis of eggshell biochar beads for superior aqueous phosphate adsorption with potential urine P-recovery, *Colloids and Surfaces A: Physicochemical and Engineering Aspects*, 2021, **622**:126589 [Crossref], [Google Scholar], [Publisher]
[50]. Zhao H., Ouyang X.K., Yang L.Y. Adsorption of lead ions from aqueous solutions by porous cellulose nanofiber–sodium alginate hydrogel beads, *Journal of Molecular Liquids*, 2021, **324**:115122 [Crossref], [Google Scholar], [Publisher]
[51]. El Allaoui B., Benzeid H., Zari N., Bouhfid R. Functional cellulose-based beads for drug delivery: Preparation, functionalization, and applications, *Journal of Drug Delivery Science and Technology*, 2023, 104899 [Crossref], [Google Scholar], [Publisher]
[52]. Gunes B., Jaquet Y., Sánchez L., Pumarino R., McGlade D., Quilty B., Morrissey A., Gholamvand Z., Nolan K., Lawler J. Activated graphene oxide-calcium alginate beads for adsorption of methylene blue and pharmaceuticals, *Materials*, 2021, **14**:6343 [Crossref], [Google Scholar], [Publisher]
[53]. Liu T., Yi S., Liu G., Hao X., Du T., Chen J., Meng T., Li P., Wang Y. Aqueous two-phase emulsions-templated tailorable porous alginate beads for 3D cell culture, *Carbohydrate polymers*, 2021, **258**:117702 [Crossref], [Google Scholar], [Publisher]
[54]. yousri Eweida B., El-Moghazy A.Y., Pandey P.K., Amaly N. Fabrication and simulation studies of high-performance anionic sponge alginate beads for lysozyme separation, *Colloids and Surfaces A: Physicochemical and Engineering Aspects*, 2021, **619**:126556 [Crossref], [Google Scholar], [Publisher]
[55]. Khusna L.N., Yulianti E., Khoiroh L.M., Istighfarini V.N. *International Conference on Engineering, Technology and Social Science (ICONETOS)*, **2021**:383 [Crossref], [Google Scholar], [Publisher]
[56]. Córdova B.M., Venâncio T., Olivera M., Huamani-Palomino R.G., Valderrama A. Xanthation of alginate for heavy metal ions removal. Characterization of xanthate-modified alginates and its metal derivatives, *International journal of biological macromolecules*, 2021,

169:130 [Crossref], [Google Scholar], [Publisher]
[57]. Wang T., Li B., Si H. Preparation of Regenerated Cellulose Bead and Its Coating With Cyclodextrins, *Cellulose Chemistry and Technology*, 2013, **47**:37 [Google Scholar], [PDF]
[58]. Rehman N., de Miranda M.I.G., Rosa S.M., Pimentel D.M., Nachtigall S.M., Bica C.I. Cellulose and nanocellulose from maize straw: an insight on the crystal properties, *Journal of Polymers and the Environment*, 2014, **22**:252 [Crossref], [Google Scholar], [Publisher]

How to cite this manuscript: Eny Yulianti, Lilik Miftahul Khoiroh, Rif'atul Mahmudah, Sindi Puspitasari, Faiqotul Himmah, Tzu-Teng Huang, Imtiaz Ali Laghari, Ahmad Zikri, Mohammad Abdullah, Rahadian Zainul, Tarek A. Elkhooly. Extraction of Cellulose from Bagasse for the Synthesis of Alginate:Cellulose Porous Beads. *Asian Journal of Green Chemistry*, 8(3) 2024, 278-295.
DOI: 10.48309/AJGC.2024.440660.1475